RESEARCH ARTICLE

Comparing Halogen Atom Abstraction Kinetics for Mn(I), Fe(I), Co(I), and Ni(I) Complexes by Combining Electroanalytical and Statistical Modeling

Tianhua Tang, Nathan C. Friede, Shelley D. Minteer,* and Matthew S. Sigman*

[a] T. Tang, N. C. Friede, Prof. S. D. Minteer, Prof. M. S. Sigman
Department of Chemistry, University of Utah
315 South 1400 East, Salt Lake City, Utah 84112 (USA)
E-mail: minteer@chem.utah.edu
sigman@chem.utah.edu

Supporting information for this article is given via a link at the end of the document.

Abstract: First-row transition metal complexes have garnered attention due to their ability to activate aliphatic halides for catalytic cross-coupling reactions. However, mechanistic investigation of these systems is challenging as a consequence of difficulties associated with preparing the relevant metal complexes and the resultant poor stability of such intermediates for subsequent analytical interrogation. In this context, we have developed a platform to rapidly measure kinetic data using electroanalytical methods, which facilitates a wide range of physical organic studies. As a result, we have investigated and compared the reaction of benzyllic halides with electrogenerated Mn^{I}(PyBox)Cl, Fe^{I}(Pyrox)OTf, Co^{I}(Pyrox)Br, Co^{I}(PyBox)Br, Ni^{I}(Phox)Br complexes. The experimental results support a unified inner-sphere halogen atom abstraction mechanism for these different complexes while also providing the ability to directly compare through multivariate linear regression analyses the subtle differences imparted by metal/ligand combinations. The information gleaned by this study has implications why certain metal complexes are matched to oxidative addition processes relevant in catalytic processes.

Introduction

As the community continues to explore the use of earth-abundant first-row transition metals in redox catalysis of electrophilic cross-coupling reaction partners,[1] an in-depth understanding of the mechanistic processes involved is required to enable a rational approach to reaction development.[2] Although significant progress has been reported, experimental mechanistic studies remain a challenge.[3–10] This is a consequence of the synthetic difficulty in accessing discrete intermediates who both retain reactivity towards the substrate of interest and the requisite stability for adequate characterization.[4–8] This complexity also can be manifested in measuring essential kinetic data for these processes, which is often a requirement to gain insight into the controlling events that can influence catalysis.[9,10] In this context, we have recently reported the use of a series of electroanalytical methods to analyze several ligated Co(I) complexes in the activation of a wide range of benzylic halides.[11-13] These tools provided access to rapid kinetic data collection allowing for the application of traditional physical organic experiments (e.g., kinetic isotope effects, Hammett studies), combined with statistical modelling of catalyst/substrate descriptors to provide insight into the mechanism of substrate activation. Specifically, analysis of a pyridine-oxazoline (Pyrox) bidentate ligand set,[11] resulted in the proposal of a halogen atom abstraction mechanism for the resulting Co(I) complexes. In contrast, investigation of a Co(I) complex bearing two 2,6-bis(pyrazol-1-yl)pyridine (BPP) tridentate ligands[12] provided evidence of an alternative mechanism of an outer-sphere electron transfer pathway of benzylic halides. A more recent study by Liu and Diao et al disclosed a halogen-atom dissociation mechanism for the activation of alkyl halides by a catalysis-relavent square planar Ni(I)(BPy) complex.[9c] The central outcome of these studies was two-fold: 1) the electroanalytical tools are enabling due to their ability to be rapidly applied to new systems, and 2) the kinetic data

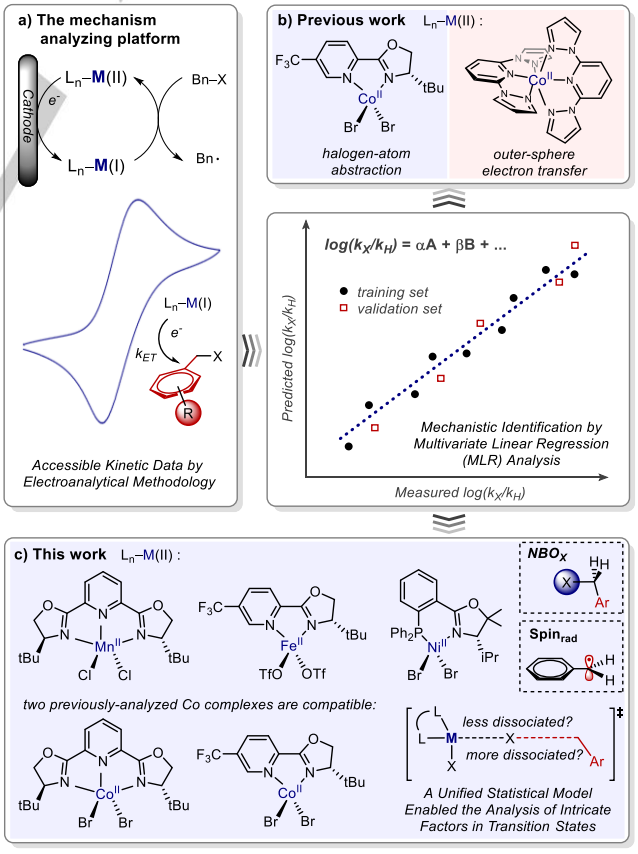

Scheme 1 Sumary of our previous and present work

and resulting statistical modelling can be used in concert to determine subtle mechanistic features not available through the study of a singular substrate or catalyst.

Thus, we envisioned a significant expansion of this platform in the study of other low-valent metals bearing nitrogenous ligands and comparing the kinetic profiles to reveal how different ligand/metal combinations activate benzylic halides. Herein we report the investigation of a Mn(I) complex bearing a pyridine-bisoxazoline (PyBox) ligand, an Fe(I) complex bearing a pyridine-oxazoline (Pyrox) ligand, and a Ni(I) complex bearing a phosphinooxazolines (Phox) ligand (Scheme 1.c). The resulting analysis not only supports a halogen atom abstraction mechanism for all complexes, but we also discovered a unified statistical model capable of describing Mn(I), Fe(I), Ni(I) and two previously-analyzed[11b,12] Co(I)'s halogen atom abstraction kinetics.[14] The interpretation of the statistical models allows for a more precise understanding of the activation process. Specifically, classification of the complexes is achieved by evaluating the coefficients determined in the statistical models wherein the Mn(I) complex is distinct from the other complexes evaluated. The successful unification of the overall mechanistic patterns presents a means to generalizing alkyl halide activation in first-row organometallic systems.

Results and Discussion

Voltammetric Studies of the Mn(PyBox)Cl_2, Fe(Pyrox)$(OTf)_2$, and Ni(Phox)Br_2 Complexes: Cyclic voltammetric (CV) measurements were utilized to initially survey the reversibility of the redox processes for various manganese, iron, and nickel complexes of commonly-used ligands in transition metal catalysis.[15] In particular, we identified a manganese complex bearing a pyridine-bisoxazoline (PyBox) ligand, an iron complex bearing a pyridine-oxazoline (Pyrox) ligand, and a nickel complex bearing a phosphino-oxazolines (Phox) ligand that meet the requisite reversibility for the substrate profiling analysis (Figure 1). As alluded to above, these ligands have been used widely in asymmetric catalysis, although these particular complexes have not been extensively explored in the context of alkyl halide activation previously.[16] Nickel-Phox-mediated cross-electrophile coupling has been previously reported but the mode of substrate activation was not investigated.[16d] The CVs of Mn(PyBox)Cl_2 were measured with a solution containing a 1:1 stoichiometry of $MnCl_2$ and PyBox ligand.[17] At the scan rates of 0.10, 0.05, and 0.02 V s^{-1}, a redox couple with a $E_{1/2}$ = −1.67 V (vs Fc/Fc^+) was defined, as is shown in Figure 1.a. To probe the speciation of the Mn complex, we conducted a square-wave voltammetric study (SWV, Figure 1.b). The peak potential of the major peak was found at −1.67 V (vs Fc/Fc^+), consistent with the clean formation of a single complex with 1 equiv. of ligand. We designated this peak response as the Mn(II)/Mn(I) redox cycle initiating from a mono-ligated Mn(PyBox)Cl_2 complex. The CVs of the iron complex were measured in a similar manner with the same equiv. of Fe$(OTf)_2$ and Pyrox ligand and the reversibility of Fe(II)/Fe(I) redox cycle (−1.49 V vs Fc/Fc^+) using slow scan rates is shown in Figure 1c.[17] The following square-wave voltammetric study was conducted, shown in Figure 1d, where the peak responses at −1.49 V and −1.99 V (vs Fc/Fc^+) were designated as the Fe(II)/Fe(I) and subsequent Fe(I)/Fe(0) redox cycles starting from the mono-ligated Fe(Pyrox)$(OTf)_2$ complex. Similarly, it forms a single

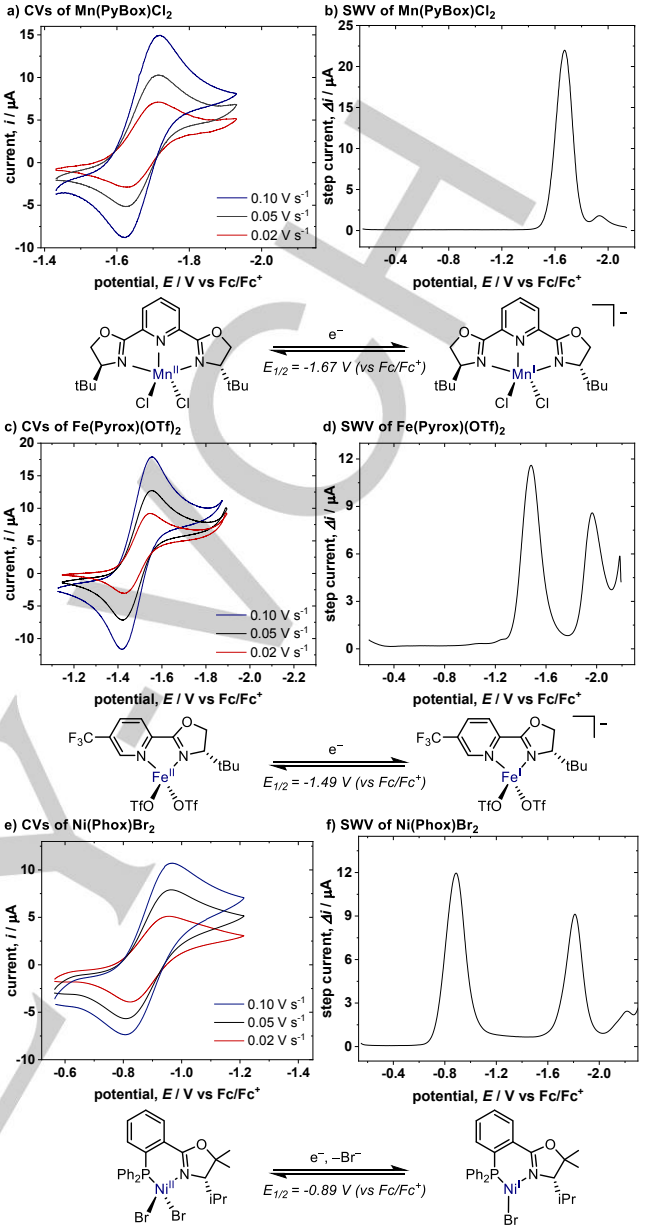

Figure 1. Representative CVs of (a) 1.0 mM $MnCl_2$ with 1.0 mM PyBox ligand, (c) 1.0 mM Fe$(OTf)_2$ with 1.0 mM Pyrox ligand, and (e) 1.0 mM $NiBr_2 \cdot 3H_2O$ with 1.0 mM Phox ligand at varying scan rates. SWVs were performed under the same condition (b) as (a) , (d) as (c), and (f) as (d). All CVs are measured in a 100 mM solution of Bu_4NPF_6 in acetonitrile, using a 0.071 cm^2 boron-doped diamond working electrode, plotted from the second scan in polarographic notation with positive currents corresponding to reduction. All SWVs are measured with pulse height = 20 mV, pulse width = 20 ms (50 Hz), and a step height = 2 mV.

complex by mixing the same equiv. of $NiBr_2 \cdot 3H_2O$ and the Phox ligand, as indicated by its CV and SWV (Figure 1e, f). The peak response at −0.89 V (vs Fc/Fc^+) in both CV and SWV was thus designated as a Ni(II)/Ni(I) reduction from a mono-ligated Ni(Phox)Br_2 complex.[17] More discussion on the ligation and speciation of both complexes is documented in the supporting information.

Reaction of Benzyl Bromide with Low-Valent Mn, Fe, and Ni Complexes: Upon the addition of 1 equiv. of benzyl bromide, the cyclic voltammograms of Mn(PyBox)Cl_2, Fe(Pyrox)$(OTf)_2$, and Ni(Phox)Br_2 demonstrate some features of irreversibility

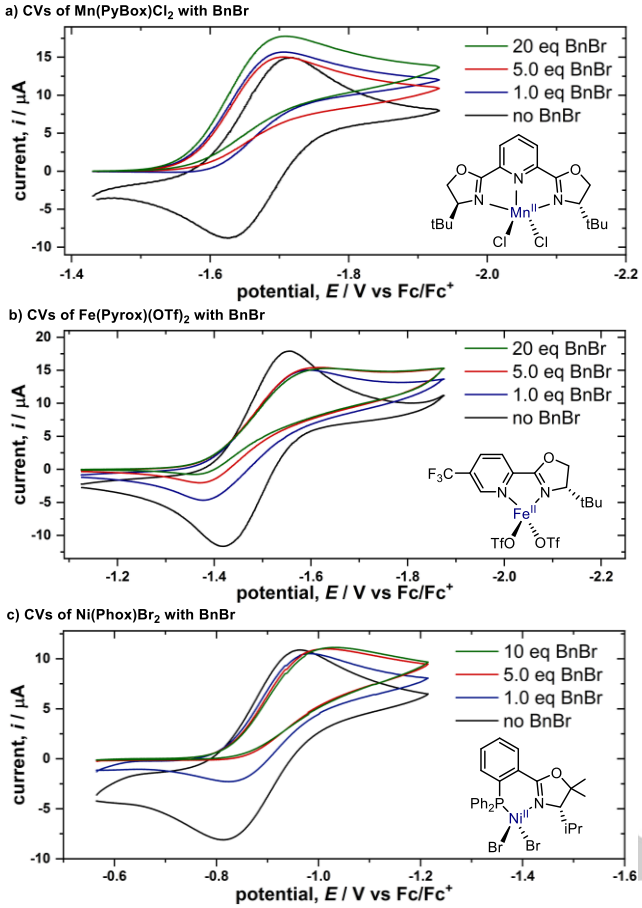

Figure 2. CVs run with (a) 1.0 mM $MnCl_2$ with 1.0 mM PyBox, (b) 1.0 mM $Fe(OTf)_2$ with 1.0 mM Pyrox, and (c) 1.0 mM $NiBr_2{\cdot}3H_2O$ with 1.0 mM Phox ligand at varying equivalents of benzyl bromide in a 100 mM solution of Bu_4NPF_6 in acetonitrile, using a 0.071 cm^2 boron-doped diamond working electrode at a scan rate of 0.10 V s^{-1}. All CVs are from the second scan.

(Figure 2.a, b and c, blue trace). Increasing the concentration of benzyl bromide resulted in increased irreversibility in their CVs. These observations indicate a chemical reaction with benzyl bromide by the electrochemically reduced Mn(I), Fe(I), Ni(I) complexes. If the Mn(II), Fe(II), or Ni(II) generated after the chemical reaction underwent a subsequent electrochemical reduction, one would expect to observe a sequential increase in current as more benzyl bromide was added, consistent with a catalytic process.[18] The measured current under an ideal catalytic situation should result in the peak cathodic current being proportional to the square root of substrate concentration.[19] However, the Mn complex's CVs (Figure 2.a) displayed an increased current with the addition of 20 equiv. benzyl bromide but far from the theoretical increase one would expect for a catalytic current.

Similarly, CV analysis of the Fe and Ni complexes (Figure 2.b and c) resulted in no observable increase in current with higher concentrations of benzyl bromide. The lack of a catalytic current for these examples is consistent with a second chemical step consuming the complex, which retards the catalysis.[20] In accordance with our previous studies,[11b] we propose a putative competitive radical rebound of the benzylic radical to the metal (at either 1+ or 2+ oxidative state or both), resulting in an ECC type mechanism (electrochemical reduction, 'E', followed by a chemical step of benzyl bromide reduction by the complexes, 'C', then a chemical step of benzylic radical rebound to the complexes, 'C',). However, the exact nature of the radical generation through either an inner-sphere or outer-sphere electron transfer pathway is not clear for the Mn(I), Fe(I), and Ni(I) complexes.

Hammett Studies: In order to investigate the mechanism of the oxidative addition/substrate activation by the Mn(I), Fe(I), and Ni(I) complexes with benzyl bromide, we conducted kinetic studies by measuring the rate constants for the chemical reaction between the low-valent metal complexes and a panel of benzyl bromide substrates through cyclic voltammetry.[11–12] The distinct kinetic behavior displayed by electronically and sterically varied benzyl bromides enables multiple physical organic experiments to be performed. This provides the basis for further identification of the mechanism for the complexes under study.

After determining the relative rate constants for a variety of *para*-substituted benzyl bromides **1–10**, a linear free energy relationship analysis was performed using Hammett σ parameters.[21] Correlations were built and compared for substrate behavior between the $Mn(PyBox)Cl_2$, $Fe(Pyrox)(OTf)_2$, $Ni(Phox)Br_2$, and the reported $Co(Pyrox)Br_2$[11b] and $Co(PyBox)Br_2$[12,22] complexes (Figure 3). The Hammett plots of these three complexes displayed a broken or curved pattern between substrates with electron-rich groups (best correlated with σ^+) and those with electron-deficient groups (best correlated with σ^-). The rationalization was described in our previous study on the $Co(Pyrox)Br_2$ complex (Figure 3.c), wherein the curved pattern is indicative of a halogen atom abstraction mechanism. The reaction is facilitated by the stabilization of radical character on the substrates' benzylic carbon by either electron-rich or electron-deficient substituents,[11b] of which the same effect was disclosed by Liu and Diao's study.[9c] As a result, the curved Hammett response for the new complexes suggests an inner-sphere halogen atom abstraction mechanism of the benzylic halides.

With the overall curved trend of the Hammett plots shared by Mn, Fe, Ni, and two Co complexes, there are key differences, including a significant difference between ρ values for σ^- for Mn (2.60) and Ni (2.14) as compared to Fe (0.60) and Co (0.79 with Pyrox and 1.22 with PyBox).[23,24] Other observations include that substrate **4** appears to be anomalous in the Hammett correlation for Mn but not for Fe, Co, and Ni. These data could indicate that a different activation pathway is operative for Mn in comparison to Co, Fe, and Ni. However, a more explicit rationale is difficult to ascertain from the Hammett plots alone.

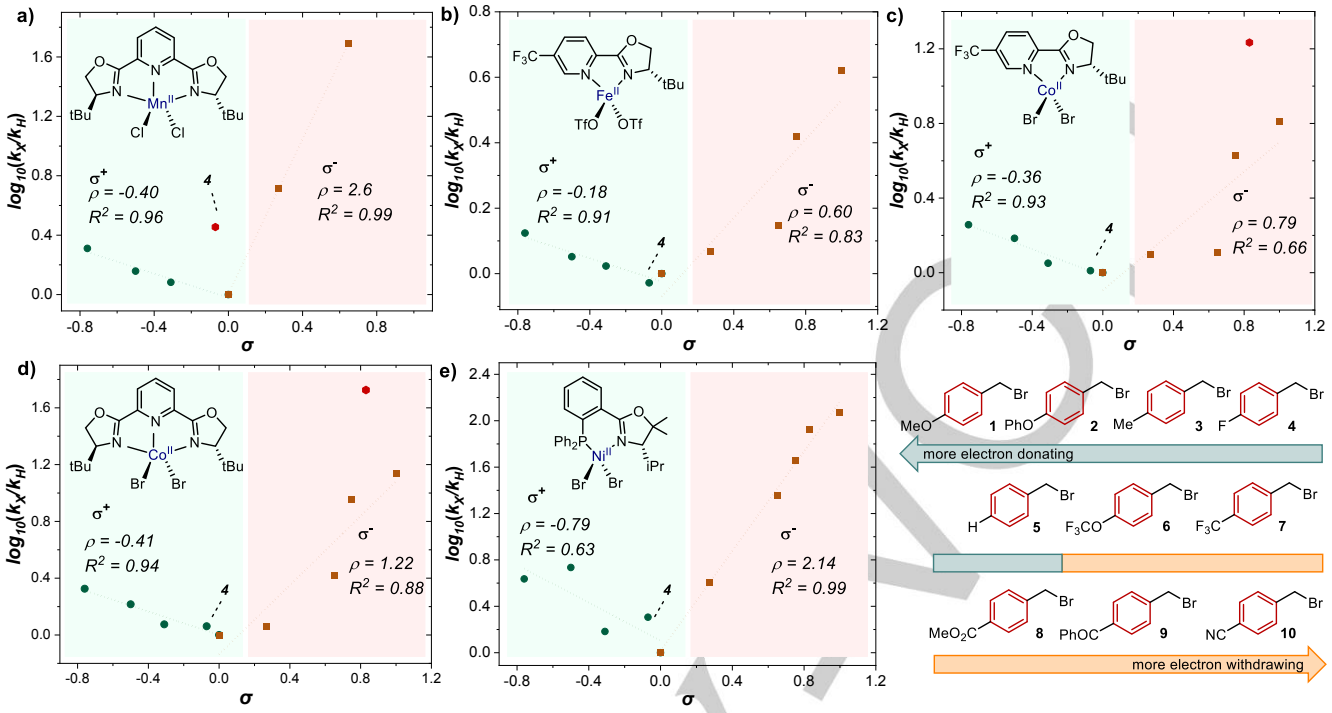

Figure 3. Hammett plots for activation of benzyl bromides by the electrochemically generated (a) Mn^{I}(PyBox)Cl, (b) Fe^{I}(Pyrox)OTf, (c) Co^{I}(Pyrox)Br, (d) Co^{I}(PyBox)Br, and (e) Ni^{I}(Phox)Br. The red circles in (a) represent substrate **4** while the re circles in (c) and (d) represent substrate **9**. All three plots use kinetic data from the same substrate set, shown on the bottom right of the figure, but the data in (a) with substrate **8**−**10** and in (b) with substrate **9** are lacked due to complete irreversibility in their CVs from which we were not able to obtain rate constants. The lines with negative correlations use σ^{+} values, while the lines with positive correlations use σ^{-} values.[21]

Secondary Substrate Effect Studies: To gain further mechanistic insight into the putative halogen atom abstraction mechanism, we conducted a kinetic study by comparing the rate constants between primary and secondary benzylic halide substrates.[11b,12] The Mn^{I}(PyBox)Cl, Fe^{I}(Pyrox)OTf, Co^{I}(PyBox)Br[22], and Ni^{I}(Phox)Br complexes were evaluated using secondary (*2°*) and primary (*1°*) brominated substrates **11**−**17** and chlorinated substrates **18**−**21** to test the impact of these changes on the substrate structure. As shown in Table 1, the brominated substrates react with Mn, Fe, Co, and Ni complexes. In contrast, the chlorinated substrates are not observed to react with Fe, Co, and Ni complexes upon 1:1 equivalency of complex to substrate concentration. In contrast to the general similarities in the Hammett study, the comparison of the dist substrate types reveals different patterns for the Mn complex and the other three complexes. Specifically, the Mn complex reacts faster with primary benzylic bromides, while the Fe, Co, and Ni complexes react faster with the secondary substrates. The latter observation is in agreement with our previous analysis of Co^{I}(Pyrox)Br's activation of benzyl halides,[11b] wherein faster rates with secondary substrates were rationalized to occur due to enhanced radical character stability in the transition state. This again suggests that the Mn complex has unique mechanistic features relative to the other systems.

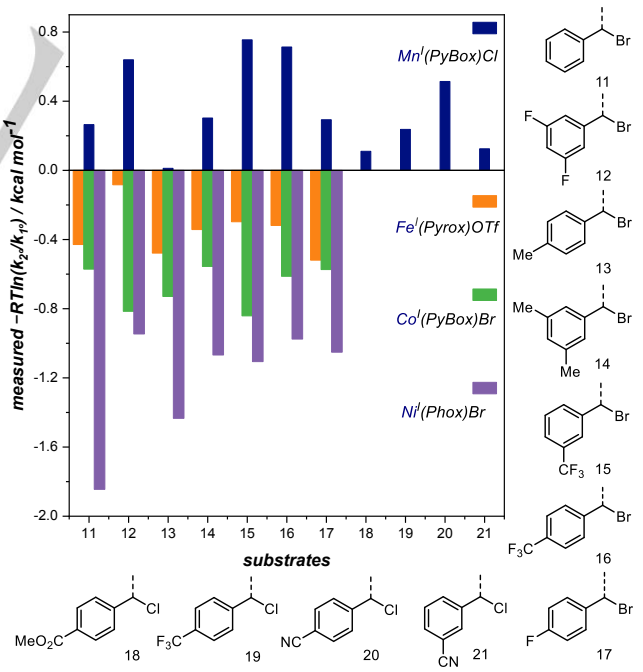

Table 1. Secondary Substrate Effect Study: Secondary substrate effect for Mn^{I}(PyBox)Cl, Fe^{I}(Pyrox)OTf, Ni^{I}(Phox)Br, and Co^{I}(PyBox)Br complexes, quantified by the difference in activation energy by secondary over primary substrate.

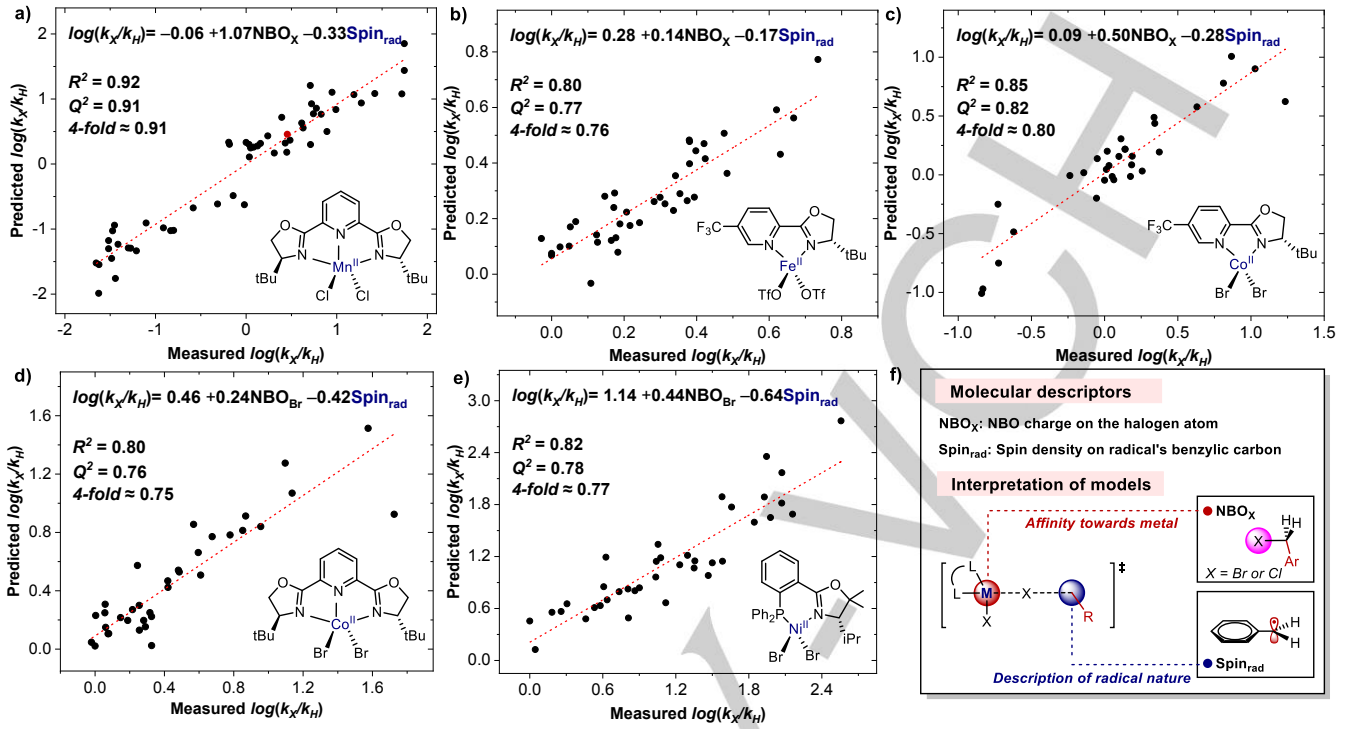

Figure 4. Multivariate linear-regression analysis of substrates' kinetic data with substrate's halogen atom's NBO charge (*NBO*$_X$) and radical's spin density (*Spin*$_{rad}$) for (a) Mn^{I}(PyBox)Cl, red circle represents the Hammett outlier substrate **4**, (b) Fe^{I}(Pyrox)OTf, (c) Co^{I}(Pyrox)Br, (d) Co^{I}(PyBox)Br, (e) Ni^{I}(Phox)Br. (f) Description of molecular descriptors, and interpretation of models within Figure 4.

Parameterization of Substrates and Statistical Modeling of Kinetic Data: The identification of the benzyl halide activation pathway by the Mn^{I}(PyBox)Cl, Fe^{I}(Pyrox)OTf, and Ni^{I}(Phox)Br complexes was complicated by the contradictory observations in the Hammett and substrate effect studies. We argue that such a conflict imposed by those analyses suggests either distinct mechanisms for the Mn from other complexes or the existence of other intricate factors[25] in the transition state. As a result, we conducted further kinetic studies with the assistance of multivariate linear-regression (MLR) analysis to provide a greater level of precision to understanding the factors governing the mechanism.[14] This technique is capable of statistically translating experimental results into interpretable mechanistic consequences.[26,27] To aid the MLR analysis, we evaluated a wider range of substrates, which could be classified into four groups: (1) primary benzyl bromides including those with ortho-substituents, (2) secondary benzyl bromides, (3) primary benzyl chlorides including those with *ortho*-substituents, and (4) secondary benzyl chlorides. For Mn^{I}(PyBox)Cl and Co^{I}(Pyrox)Br, all 4 types of substrates were tested to measure their rate constants, while for Fe^{I}(Pyrox)OTf, Co^{I}(PyBox)Br, and Ni^{I}(Phox)Br only groups (1) and (2) were tested due to lack of reactivity with benzyl chlorides.

Next, we turned to the selection of molecular descriptors to correlate to the measured kinetic data. We hypothesized the activation kinetics in this study could be perturbed by the interaction between the metal and halogen atom in the transition state. The abstraction process could be facilitated by an electron-deficient halogen atom with a larger affinity towards the electron-rich metal core. As a consequence, the partial charge on the halogen atom in the substrate according to the natural bonding orbitals was selected as a parameter (*NBO*$_X$) to describe the halogen affinity in the transition state.[28] Inspired by our previous studies of cobalt systems,[11b] the spin density according to NBO of the benzylic carbon in the radical product (*Spin*$_{rad}$) was incorporated as another essential parameter.

With both the kinetic data and selected molecular descriptors acquired, statistical models were developed. Models were selected with a focus on determining statistical correlations using the same descriptors for each metal complex. This revealed a set of bivariate models with good to excellent regression statistics in all cases (Figure 4a-c: R^2, Q^2, and *4-fold*, are over 0.75 for Mn^{I}(PyBox)Cl, Fe^{I}(Pyrox)OTf, Co^{I}(Pyrox)Br, Co^{I}(PyBox)Br, and Ni^{I}(Phox)Br). Of particular interest, substrate **4** is no longer anomalous, and by virtue of using the same descriptors for the four systems, the same general mechanism for the different complexes is suggestive (red circle in Figure 4.a). Furthermore, in contrast to the conflicted conclusion drawn by the Hammett and secondary substrate effect studies, a unified pattern accounting for substrates' kinetic behavior is afforded by the MLR analysis, where the Mn, Fe, Ni, and two Co's mechanistic models were integrated by one set of molecular descriptors (*NBO*$_X$, and *Spin*$_{rad}$), suggesting they react through the same general process. Alternatively, the C−X bond

dissociation energy (BDE) has been proposed to determine the halogen abstraction kinetics,[9c,25] thus a study of BDE as a parameter is also conducted, where the result and discussion is given in the supporting information.

In addition, the halogen's NBO charge (NBO_X) can be interpreted to describe the halogen's affinity to the metal center in the bimolecular interaction, while the benzylic radical's spin density ($Spin_{rad}$) can reflect the generation and stabilization of radical character on this carbon during the transition state, both supportive of an inner-sphere halogen atom abstraction mechanism (Figure 4.f). The Mn's model is distinctive from the others in its much larger coefficient on NBO_X (1.07) than $Spin_{rad}$ (0.33). This could indicate a less-dissociated halogen atom on the benzyl group in the transition state for the Mn catalyst compared to the other metals interrogated. If the halogen atom is fully dissociated in the transition state, one would expect to observe no correlation with NBO_X. Comparatively, Fe, Ni, and the two Co complexes could possess a transition state in which the substrate has a more dissociated feature with greater radical character on the benzylic carbon.

As detailed above, the readout for different substrate types was disclosed for the Mn complex, of which the rationalization is consistent with this analysis.[29] Characterized by the NBO_X parameter, substrate **11** (−0.03949) has a more electron-rich bromide atom with less affinity to metal than **5** (−0.02617), while **11** (0.74131) better stabilizes the radical character than **5** (0.78003) described by $Spin_{rad}$ parameter. For Mn^{I}(PyBox)Cl where NBO_X dominates the statistical model, the activation of the secondary substrate is overall unfavorable compared to the primary substrate, thus following our observation.

Conclusion

In conclusion, we have investigated the halogen atom abstraction mechanism by low-valent Mn^{I}(PyBox)Cl, Fe^{I}(Pyrox)OTf, Co^{I}(Pyrox)Br, Co^{I}(PyBox)Br, and Ni^{I}(Phox)Br complexes. The identification of their reactivity profile with benzyl halide substrates as well as the resulting mechanistic analysis was enabled by the electroanalytical techniques to rapidly measure rate data. Mechanistically, the experiments support a halogen atom abstraction mechanism for the Mn, Fe, Co, and Ni complexes, although subtle differences that could impact future reaction design are apparent. The use of multivariate linear-regression analysis was used to provide a more precise analysis of said differences wherein the parameters used and the coefficients measured in the statistical model, the halogen's NBO charge and the benzylic radical's spin density, provided the ability to forecast the proposed nature of the transition states. This study presents a blueprint for profiling disparate electrochemically active metal complexes experimentally and comparing them directly using statistical modelling. We are currently exploring how to apply these complexes with the knowledge gained in this study and exploiting these techniques in the evaluation of a wide range of metal complexes.

Acknowledgments

The authors would like to thank the National Science Foundation Center for Synthetic Organic Electrochemistry for funding (CHE-2002158). NMR results included in this report were recorded at the David M. Grant NMR Center, a University of Utah Core Facility. Funds for the construction of the Center and the helium recovery system were obtained from the University of Utah and the National Institutes of Health awards 1C06RR017539- 01A1 and 3R01GM063540-17W1, respectively. NMR instruments were purchased with the support of the University of Utah and the National Institutes of Health award 1S10OD25241-01. The authors also acknowledge Christopher Sandford for insightful discussions.

Keywords: electrochemistry • multivariate linear regression • oxidative addition

[1]. For selected reviews, see: (a) L. A. Wessjohann, G. Scheid, *Synthesis* **1999**, *1*, 1–36. (b) J. M. Concellón, H. Rodríguez-Solla, V. del Amo, *Chem. -Eur. J.* **2008**, *14*, 10184–10191. (c) T. L. Mako, J. A. Byers, *Inorg. Chem. Front.* **2016**, *3*, 766–790. (d) J. Demarteau, A. Debuigne, C. Detrembleur, *Chem. Rev.* **2019**, *119*, 6906–6955. (e) J. Choi, G. C. Fu, *Science* **2017**, *356*, eaaf7230. (f) L.-J. Cheng, N. P. Mankad, *Acc. Chem. Res.* **2021**, *54*, 2261–2274.

[2]. For selected reviews, see: (a) X. Hu, *Chem. Sci.* **2011**, *2*, 1867–1886. (b) K. Matyjaszewski, *Macromolecules* **2012**, *45*, 4015–4039. (c) J. D. Sears, P. G. N. Neate, M. L. Neidig, *J. Am. Chem. Soc.* **2018**, *140*, 11872–11883. (d) J. B. Diccianni, T. Diao, *Trends Chem.* **2019**, *1*, 830–844.

[3]. (a) N. D. Schley, G. C. Fu, *J. Am. Chem. Soc.* **2014**, *136*, 16588–16593. (b) J. B. Diccianni, J. Katigbak, C. Hu, T. Diao, *J. Am. Chem. Soc.* **2019**, *141*, 1788–1796.

[4]. (a) D. H. Hill, M. A. Parvez, A. Sen, *J. Am. Chem. Soc.* **1994**, *116*, 2889–2901. (b) S. L. Daifuku, J. L. Kneebone, B. E. R. Snyder, M. L. Neidig, *J. Am. Chem. Soc.* **2015**, *137*, 11432–11444.

[5]. J. M. Ahn, T. S. Ratani, K. I. Hannoun, G. C. Fu, J. C. Peters, *J. Am. Chem. Soc.* **2017**, *139*, 12716–12723.

[6]. (a) Q. Lin, T. Diao, *J. Am. Chem. Soc.* **2019**, *141*, 17937–17948. (b) C. L. Wagner, G. Herrera, Q. Lin, C. T. Hu, T. Diao, *J. Am. Chem. Soc.* **2021**, *143*, 5295–5300. (c) L. Ju, Q. Lin, N. L. LiBretto, C. L. Wagner, C. T. Hu, J. T. Miller, T. Diao, *J. Am. Chem. Soc.* **2021**, *143*, 14458–14463.

[7]. S. M. Rummelt, P. O. Peterson, H. Zhong, P. J. Chirik, *J. Am. Chem. Soc.* **2021**, *143*, 5928–5936.

[8]. H. Tinnermann, S. Sung, D. Csókás, Z. H. Toh, C. Fraser, R. D. Young, *J. Am. Chem. Soc.* **2021**, *143*, 10700–10708.

[9]. (a) A. Wuttig, J. S. Derrick, M. Loipersberger, A. Snider, M. Head-Gordon, C. J. Chang, F. D. Toste, *J. Am. Chem. Soc.* **2021**, *143*, 6990–7001. (b) N. A. Till, S. Oh, D. W. C. MacMillan, M. J. Bird, *J. Am. Chem. Soc.* **2021**, *143*, 9332–9337. (c) Q. Lin, Y. Fu, P. Liu, T. Diao, *J. Am. Chem. Soc.* **2021**, 143, 14196–14206.

[10]. (a) J. K. Kochi, J. W. Powers, *J. Am. Chem. Soc.* **1970**, *92*, 137–146. (b) D.-I. Zhou, J. Gao, J. F. Rusling, *J. Am. Chem. Soc.* **1995**, *117*, 1127–1134.

[11]. (a) D. P. Hickey, C. Sandford, Z. Rhodes, T. Gensch, L. R. Fries, M. S. Sigman, S. D. Minteer, *J. Am. Chem. Soc.* **2019**, *141*, 1382–1392. (b) C. Sandford, L. R. Fries, T. E. Ball, S. D. Minteer, M. S. Sigman, *J. Am. Chem. Soc.* **2019**, *141*, 18877–18889.

[12]. T. Tang, C. Sandford, S. D. Minteer, M. S. Sigman, *Chem. Sci.* **2021**, *12*, 4771–4778.

[13]. C. Sandford, M. A. Edwards, K. J. Klunder, D. P. Hickey, M. Li, K. Barman, M. S. Sigman, H. S. White, S. D. Minteer, *Chem. Sci.* **2019**, *10*, 6404–6422.

[14]. (a) K. C. Harper, M. S. Sigman, *J. Org. Chem.* **2013**, *78*, 2813–2818. (b) M. S. Sigman, K. C. Harper, E. N. Bess, A. Milo, *Acc. Chem. Res.* **2016**, *49*, 1292–1301.

[15]. (a) G. Desimoni, G. Faita, P. Quadrelli, *Chem. Rev.* **2003**, *103*, 3119–3154. (b) G. Yang, W. Zhang, *Chem. Soc. Rev*. **2018**, *47*, 1783–1810. (c) J.-Y. Guo, Y. Minko, C. B. Santiago, M. S. Sigman, *ACS Catal*. **2017**, *7*, 4144–4151. (d) G. C. Hargaden, P. Guiry, J. *Chem. Rev*. **2009**, *109*, 2505–2550.

[16]. (a) A. M. Tondreau, J. M. Darmon, B. M. Wile, S. K. Floyd, E. Lobkovsky, P. J. Chirik, *Organometallics* **2009**, *28*, 3928–3940. (b) T. Ollevier, *Catal. Sci. Technol.* **2016**, *6*, 41. (c) S. Budweg, K. Junge, M. Beller, *Chem. Commun*. **2019**, *55*, 14143–14146. (d) N. T. Kadunce, S. E. Reisman, *J. Am. Chem. Soc*. **2015**, *137*, 10480–10483.

[17]. For the rational of selection of ligands and counterions for either Mn, Fe, or Ni complex, see Supporting Information.

[18]. (a) J. M. Savéant, *Electrochim. Acta* **1967**, *12*, 999−1030. (b) C. P. Andrieux, C. Blocman, J. M. Dumas-Bouchiat, F. M'Halla, J. M. Savéant, *J. Electroanal. Chem. Interfacial Electrochem.* **1980**, *113*, 19−40.

[19]. E. S. Rountree, B. D. McCarthy, T. T. Eisenhart, J. L. Dempsey, *Inorg. Chem*. **2014**, *53*, 9983–10002.

[20]. (a) D. Lexa, J.-M. Savéant, *J. Am. Chem. Soc.* **1988**, *110*, 7617–7625. (b) C. Costentin, S. Drouet, M. Robert, J.-M. Saveant, *J. Am. Chem. Soc.* **2012**, *134*, 11235–11242.

[21]. C. Hansch, A. Leo, R. W. Taft, *Chem. Rev.* **1991**, *91*, 165–195.

[22]. To make quantitative comparison between Hammett plots for different metal complexes, the kinetic measurement for Co^{I}(PyBox)Br was conducted with 1 equiv. ligand to be consistent in conditions. In our previous study at ref.12, we used 0.5 equiv. ligand.

[23]. (a) C. Amatore, F. Pfluger, *Organometallics* **1990**, *9*, 2276−2282. (b) B. U. W. Maes, S. Verbeeck, T. Verhelst, A. Ekomié, N. von Wolff, G. Lefèvre, E. A. Mitchell, A. Jutand, *Chem. - Eur. J*. **2015**, *21*, 7858−7865.

[24]. (a) M. Foà, L. Cassar, *J. Chem. Soc., Dalton Trans*. **1975**, *23*, 2572−2576. (b) T. T. Tsou, J. K. Kochi, *J. Am. Chem. Soc.* **1979**, *101*, 6319−6332.

[25]. C. Fang, M. Fantin, X. Pan, K. de Fiebre, M. L. Coote, K. Matyjaszewski, P. Liu, *J. Am. Chem. Soc*. **2019**, *141*, 7486–7497.

[26]. (a) J. P. Reid, M. S. Sigman, *Nat. Rev. Chem*. **2018**, *2*, 290–305. (b) S. G. Robinson, M. S. Sigman, *Acc. Chem. Res.* **2020**, *53*, 289–299.

[27]. (a) J. P. Reid, M. S. Sigman, *Nature* **2019**, *571*, 343–348. (b) S. Zhao, T. Gensch, B. Murray, Z. L. Niemeyer, M. S. Sigman, M. R. Biscoe, *Science* **2018**, *362*, 670–674.

[28]. It has been reported that the donor-acceptor interaction in halogen bonding follows the Bent's rule, and can be characterized by NBO parameters: (a) S. J. Grabowski, *J. Phys. Chem. A* **2011**, *115*, 12340–12347. (b) S. J. Grabowski, *J. Phys. Chem. A* **2012**, *116*, 1838–1845.

[29]. Aside from the electronic effect, a steric effect on Mn complex's transition state is also analyzed, as detailed in supporting information.

Entry for the Table of Contents

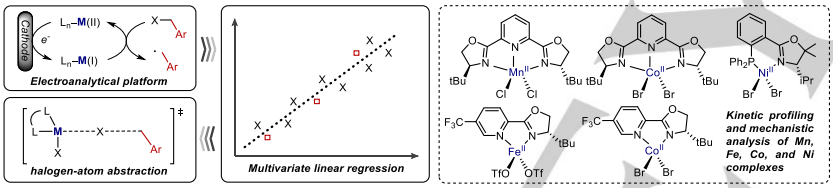

Enabled by an electroanalytical and statistical modelling platform, benzyl halide activation kinetics were profiled for five low-valent first-row transition metal complexes (Mn, Fe, Co, and Ni). A unified halogen atom abstraction mechanism was identified while subtle differences can be viewed through analysis of the statistical models.

Institute and/or researcher Twitter usernames: @sigmangroup and @MinteerLab